Predicting Radiometric Effects of a Rough Sea Surface, Whitecaps, Foam, and Spray Using SURFER 2D

Derek M. Burrage, Magdalena D. Anguelova, David W. Wang, and Joel C. Wesson

***Abstract*—Whitecap (WC) formation due to waves breaking on a wind-roughened sea surface facilitates the exchange of mass, momentum, and energy across the air–sea interface. While approximate analytical electromagnetic (EM) models paired with surface gravity wave spectra have been used to predict surface roughness emissivity enhancement, these methods do not reveal details of the response to foam, breaking wave, and WC geometry. They also ignore possible coupling between the roughness and WC emissivity effects. We report the application of a full-wave finite-difference time-domain (FDTD) EM model to investigate the separate and combined emissivity effects of specific surface roughness profiles, associated WC fields, and overlying spray. The model solves Maxwell's equations directly for an arbitrary free space and dielectric configuration. It is applied to multiple dielectric layers representing foam and spray overlying flat and rough sea surfaces. The foam layer profiles are adapted from Anguelova's *L*-band radiative transfer model and the rough surface is a statistical realization of the Kudryavtsev gravity wave spectrum. The model is also used to investigate the secondary effect of sea state on emissivity for a given mean square slope, which is the primary factor governing rough surface emissivity enhancement. The accuracy and precision of the FDTD model emissivity estimates and the detectability of WCs using *L*-band radiometry are assessed under various wind conditions, including those of tropical storm and category 1 hurricane strength. The prospects for performing Monte Carlo simulations for stronger winds and deterministic simulations of breakers with WCs of various void fractions, shapes, and scales are also considered.**

***Index Terms*—Emissivity, finite-difference time-domain (FDTD), foam, radar cross section (RCS), reflectivity, seawater, spray, whitecaps (WCs).**

Manuscript received December 4, 2018; revised April 13, 2019; accepted June 13, 2019. Date of publication August 19, 2019; date of current version September 29, 2019. This work was supported by the Office of Naval Research "Combined use of airborne reflectometry and radiometry to retrieve surface winds, waves, and wakes in tropical cyclones" research program under Program Element 0601153N. This is NRL contribution NRL/JA/7330-18-4144. *(Corresponding author: Derek M. Burrage.)*

D. M. Burrage was with the Division of Oceanography Naval Research Laboratory, Stennis Space Center, MS 39529 USA (e-mail: dmburrage425@gmail.com).

M. D. Anguelova is with the Division of Remote Sensing, Naval Research Laboratory, Washington, DC 20375 USA (e-mail: maggie.anguelova@nrl.navy.mil).

D. W. Wang and J. C. Wesson are with the Division of Oceanography, Naval Research Laboratory, Stennis Space Center, MS 39529 USA (e-mail: david.wang@nrlssc.navy.mil; joel.wesson@nrlssc.navy.mil).

Color versions of one or more of the figures in this paper are available online at http://ieeexplore.ieee.org.

Digital Object Identifier 10.1109/JSTARS.2019.2925595

I. Introduction

THE formation of whitecaps (WCs) due to waves breaking on a wind-roughened sea surface greatly facilitates the exchange of mass, momentum, and heat between the atmosphere and the ocean. It, thus, influences the processes governing weather and climate, such as the transfer of carbon dioxide, tropical convection and storm development, and ocean currents.

At moderate wind speeds (above 8 ms^{-1}), breaking waves and associated turbulence inject air at and below the sea surface, forming bubble plumes near the evolving wave crest. These plumes produce transient and sometimes persistent patches of foam, called WCs, that are visible above the surface. In higher winds, water droplets in the air form spray layers that may obscure the surface. These processes modify the apparent reflectivity and emissivity of a wind-roughened sea surface by causing changes in the physical structure and dielectric properties below, at, and above the surface. Such changes influence the response of remote sensing instruments, particularly radiometers, reflectometers, and radars of various types that probe the surface in the microwave part of the electromagnetic (EM) spectrum.

Here, we report a series of studies using the two-dimensional (2-D) version of the SURFace Emission and Reflection by Seawater And foaM ("SURFER SAM," or simply "SURFER"), finite-difference time-domain (FDTD) EM model ("SURFER 2D"; a 3-D version of the model is currently under test). These studies were performed to investigate the emissivity and the reflectivity of a wind-roughened sea surface and associated breaking waves and WCs represented by embedded foam patches. Details of the development and validation of the 1-D and 2-D versions of this model, and examples of their applications, are given in [1], which considers the qualitative effects of WCs, foam, and spray on emissivity. The applications show that an overlying spray layer obscures the sea surface and WCs to the point where they become undetectable with conventional *L*-band microwave radiometers and reflectometers.

Recent experience in retrieving ocean winds using *L*-band radiometers on the SMOS [2], aquarius\SAC-D and SMAP [3] satellites, and *L*-band reflectometers flown on the TechDemoSat-1 and cyclone global navigation satellite system (CYGNSS) constellation [4] satellites have highlighted both the potential challenges and benefits of these technologies, particular when observing storms. Key issues concern the emissivity effects of surface roughness, foam patches or WCs, and spray on

wind, temperature, and salinity retrieval algorithms, particularly as a function of increasing wind speed.

The need to correctly estimate the effects of breaking waves and associated WCs on emissivity, which progressively increase in size and areal coverage as wind speeds increase to hurricane strength, provides the primary motivation for this paper. The emissivity and reflectivity measurements made using these technologies are closely related to the mean square slope (MSS) of the sea surface, which is directly related to wind stress, and indirectly related to wind speed (through the drag coefficient). However, it has been found that sea state, which may be variously described in terms of wave height and period, fetch and duration, or wave age [5], [6], and more generally frequency and wavenumber spectrum (e.g., [7]–[9]), has a controlling influence on the *L*-band sensor response to MSS. This dependence provides additional motivation for this paper, which includes an exploration of the effects of surface gravity waveform, and associated elevation and slope distributions (represented in physical or spectral space) on emissivity, *e,* and reflectivity, *r*.

As described in [1], the foam layer geometry and void fraction profiles employed in the 1-D radiative transfer model (RTM) of Anguelova and Gaiser [10] were adopted to specify the foam dielectric properties in the FDTD model. However, the physical principles and EM solution methods employed in the two models are very different. Unlike the 1-D RTM, SURFER 2D solves Maxwell's equations directly for an arbitrary 2-D free space and dielectric configuration. Generalizing the foam layer structure to a 2-D space using FDTD allows WCs of specified shape (in the vertical plane) and of finite horizontal extent to be modeled. SURFER features an accurate EM plane wave source with highly absorbing boundary conditions to minimize spurious reflections and an auxiliary near-to-far-field transformation for computing bistatic radar cross sections (BRCS). Computing BRCS allows both *r* and *e* to be computed by integrating over the upper half space, making the FDTD model useful for both radiometry and reflectometry applications. Optional targets include idealized perfect electric conductor (PEC) layers of simple geometry, and multiple dielectric layers of constant or varying thickness, with either uniform or continuously varying dielectric properties. In the SURFER runs reported here, such layers are used to represent seawater having a flat or wind-roughened surface, with continuous foam cover or patches of embedded foam (WCs) and, optionally, overlying spray.

The simulation techniques follow those of previous FDTD studies with applications to rough surface scattering, including floating or overlying objects. FDTD 2-D models were employed by Hastings *et al.* [11]–[14] with domain electrical sizes up to $\sim$200 times the EM wavelength, λ, and typically recommended cell sizes of $\lambda/10$ or $\lambda/20$. Most models were forced by a monochromatic incident source, but Li *et al.* [14] employed a pulsed source and the auxiliary differential equation FDTD method to study the frequency response up to *L*-band. In all these 2-D cases, comparisons with integral equation or method of moments (MoM) solution demonstrated the accuracy of the FDTD method with close agreement for incidence angles from 0° up to 45° or higher. Either PEC or dielectric targets and rough sea surfaces consistent with wind speeds of 3 or 5 ms^{-1} were modeled. To determine BRCS, Monte Carlo (MC) simulations with ensembles of between 10 and 50 runs were typically performed. Rough sea surface heights were Gaussian distributed, with either a single-scale Gaussian or multiscale Pierson–Moskowitz, surface gravity wave power spectrum. Models of either one or two homogeneous seawater layers bounded by rough surfaces were constructed. Studies [15]–[17] employed 3-D FDTD models with square horizontal domains of size 10–26 λ. The 2-D and 3-D models presented in [17] showed a similar response, but the former exhibited finer backscatter structure with enhanced specular reflection, attributed to the infinite extension of the target in the direction orthogonal to the scattering plane. Models were run in single or dual polarization, and some cross-polarized BRCS results were also reported. Studies [13] and [18] used message passing parallel processing methods. Investigations of the effects of objects positioned above a rough sea surface included a small (7 λ squared) 3-D model [17] and 2-D models of 180 λ length [19], [20], while Li *et al.* [21] modeled a ship of 27 λ wide by 18 λ high floating on a rough surface of length 260 λ. These last three FDTD models agreed closely with MoM at incidence angles up to and even exceeding 60°. The models showed the rough surface dominated the response, but that increased object size enhanced the backscatter and smoothed out the specular reflection.

This study extends the 2-D modeling approach presented in [11]–[14] by adding several new features. SURFER 2D employs a more realistic (not merely Gaussian) wind-wave spectral model [7], and a homogeneous seawater layer modified with either a continuous overlying foam layer or embedded foam patches simulating WCs (forming partly submerged dielectric targets). A spray layer is optionally superimposed on these structures. Foam and spray dielectric layer properties are specified using vertical void fraction profiles, representing the fraction of air present, as a function of depth, in foam bubble plumes, and spray aerosols, respectively. Domains of width up to 1200 λ were used, depending upon wind speed (which ranged up to 35 ms^{-1}) and corresponding peak wave length. A realistic gravity wave power spectrum [7] was used to define rough surface MC realizations for ensembles of up to ten runs (depending on wind speed). To mitigate staircasing errors that can arise when rectangular cells are used to represent curved surfaces [23], convergence tests were performed with decreasing cell size. Based on these tests, and to improve accuracy, maximum cell sizes of $\lambda/42$ were specified.

As in the previous studies, comparisons with a MoM code for simple PEC and dielectric configurations with flat and rough surfaces (J. Ouellette, personal communication) showed close agreement, except at near-grazing angles of incidence. A focus on *L*-band ($\lambda\sim$21 cm) allows scattering due to individual, $\sim$1 mm or less, water droplets above the sea surface, and air bubbles below it, to be ignored, while the bulk dielectric properties and EM effects of spray aerosols and bubble plumes, such as attenuation and reflection, are fully accounted for using representative void fraction profiles. Small, $\sim$1 cm scale, surface topography features such as capillary waves can also be omitted (by lightly smoothing the surface topography profile). The FDTD solution of Maxwell's equations in SURFER then allows

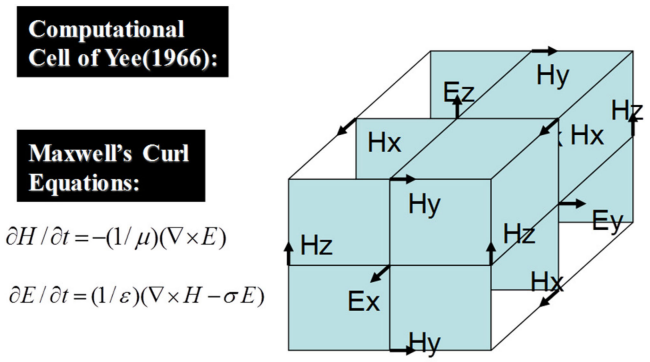

Fig. 1. Yee cell [22] employed in most FDTD algorithms to solve Maxwell's curl equations. The divergence equations (not shown) are satisfied automatically by this cell configuration.

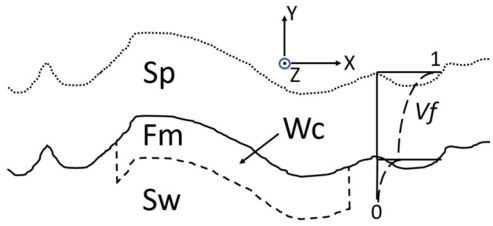

Fig. 2. Model configuration showing multiple dielectric layers representing foam (Fm) or whitecaps (Wc) and spray (Sp) overlying a rough seawater (Sw) layer. Representative void fraction (*Vf*) profiles are shown for Sp and Fm layers. The model coordinate frame is also shown.

single- and multiple-surface scattering, volume scattering due to foam, and spray and edge diffraction of WCs to be modeled, at resolutions of ∼1 mm −1 cm, consistent with grid size and available computing resources.

Section II describes the FDTD model simulation methods and model validation (the reader is referred to [1] for further details). Section III describes the results of models simulating the separate and combined effects of flat and rough seawater surfaces with embedded foam or WCs and overlying spray. A systematic study of the emissivity effects of the wind-roughened sea surface and associated WCs under increasing wind speed up to tropical storm intensity is presented. We then investigate the effects of laboratory generated waves exhibiting nonlinearities producing asymmetric and breaking waves. Finally, various linear (monochromatic) and nonlinear narrow to broad-banded surface elevation waveforms are synthesized with MSS values matching the lab waves, so secondary effects of sea state on emissivity can be isolated from the dominant influence of MSS. Section IV discusses findings and draws conclusion.

II. Methods

A. Simulation Methods

SURFER is based on the FDTD algorithms of Yee [22], Taflove and Hagness [23], and others cited therein. The model, written in highly vectorized custom MATLAB code, runs efficiently on an eight-core PC workstation with 24 GB of RAM, and optionally with a GPU. The code solves Maxwell's first-order coupled linear electric (E) and magnetic (H) field equations using the second-order explicit FD procedure on a space lattice with the Yee [22] unit cell (see Fig. 1). Cartesian E and H field component locations are staggered in space with leap FROG computation of E and H in time. Square cells used in the model with cell sizes of $dx = 2$ mm or 5 mm, depending on the application, easily resolve the EM wavelength $\lambda \sim 20$ cm at L-band, by at least a factor of 20. The time step is specified so it meets the Courant stability criterion [23].

The model features perfectly matched layer (PML) absorbing boundaries, a plane EM wave generator that utilizes the total field/scattered field (TFSF) formulation, and a near-to-far field transformation (NTFT) from which BRCS and far-field emissivity are computed [24]. It currently operates in transverse magnetic mode with respect to z (TMz), with the electric Ez component, directed out of the page, i.e., in horizontal polarization (H-Pol) relative to the horizontal sea surface target, and the orthogonal magnetic Hy and Hx components directed upward and to the right, respectively, consistent with the model's right-handed Cartesian frame [see Fig. 2]. The target is optionally a PEC or dielectric seawater layer. Unless stated, otherwise, the seawater temperature, T, and salinity, S, are 20 °C and 34 psu, respectively, the dielectric model is [25], and the incident wave frequency is $1.413 - 10^9$ Hz ($\lambda = 21$ cm).

Throughout this paper, we first probe the surface using a plane wave source to determine its effective reflectivity, r. This is done by analyzing the scattered field (SF) to determine the BRCS. We then integrate BRCS over the upper half plane to deduce r and use *Kirchhoff's* energy conservation law to deduce the effective surface emissivity, $e = 1 - r$. Hereafter, when, for brevity, we refer to emissivities obtained from simulated reflectivity, application of the above procedure is implied.

B. Application

The model is applied to multiple dielectric layers representing foam or WCs and optionally sprays overlying a rough sea surface. The WCs are represented by foam patches embedded in the surface (see Fig. 2). The WC adopts the shape and levels of that portion of the smooth or rough sea surface that it replaces, so there are no sea surface height discontinuities, even if both surfaces are rough. While, in contrast, a continuous foam or spray layer is laid on top of the sea surface (and any embedded WCs), it nevertheless conforms to the original sea surface shape. Whether continuous or patchy (comprising WCs), the foam layer's dielectric properties are determined using the RTM foam layer structure. This has a void fraction, *Vf*, profile following a specified exponential or power law, and a refractive mixing rule is used to determine the complex dielectric constant of the foam as a weighted combination of values for seawater and air [10]. The WCs, if present, may be centered in the domain or randomly distributed across the rough sea surface.

For an overlying spray layer, we experimented with two configurations. The first simply adopts the foam RTM profile configuration [10], but assigns an exponentially varying *Vf* profile representing spray under specific wind conditions. The second

employs a newly developed spray layer model [26] based on a power law water content profile with the layer height proportional to the gravity wave height. The refractive mixing rule [10] is used in both configurations.

The rough sea surface profile is a statistical realization of the Kudryavtsev gravity wave spectrum model [7]. Alternative spectral models are available including the widely adopted Elfouhailly *et al.* model [8] and the advanced spectral model of Hwang *et al.* [9], among others. The MSS [7], and WC coverage and scale [27], [28] are prescribed empirically for given wind speeds.

Model runs were performed using an incident *L*-band plane wave reflecting off a flat or wind-roughened surface for wind speeds up to 35 ms^{-1}. In selected cases, an overlying spray layer was added to assess its effects in obscuring sea surface roughness or WC effects. To study wind speed dependent WC coverage (without overlying spray), WC location, and scale were specified for winds up to 20 ms^{-1}, these being of tropical storm force, and close to the 24 ms^{-1}, upper range limit of current empirical WC coverage models.

After application of the NTFT and BRCS algorithms [23], [24], the resulting emissivities, derived from the power ratio of the simulated scattered and incident fields, were compared with predictions from the analytical small-slope approximation/small parameter method (SSA/SPM) EM model [29], [30] run using the same wave spectrum [7] and the foam emissivity model [31]. The accuracy and precision of model emissivity estimates, i.e., the roughness emissivity increment, and the detectability of WCs using *L*-band radiometry are assessed under these conditions.

C. Validation

The FDTD model was first validated by comparing simulated *r* and corresponding *e* values with those predicted by the emissivity model in [25] for specular reflection from two different targets: a PEC flat plate and a flat seawater layer (without spray or foam) over a range of incidence angles. Close agreement was found, except near grazing incidence angles exceeding 75° [1].

Comparisons were also made between RTM [10] and SURFER 2D using the same foam layer structure as [10, Fig. 13], and the Camps *et al.* [32] laboratory data and their foam emissivity model [1]. FDTD and RTM model parameters mimicked the laboratory experimental parameters. SURFER 2D mean *e* deviations for incidence angles ranging from 25° to 50° agreed with RTM within 7% and with the lab data within 10%. The FDTD model was also run for three PEC rough surface realizations of the gravity wave spectrum [7]. Results agreed closely with those obtained using an independent MoM code (J. Ouellette, NRL Remote Sensing Division, pers. comm.), giving confidence that SURFER could be applied to more complex, rough surface, geometries not modeled by RTM.

III. Results

After validation, SURFER 2D was run to study the reflectivity, and hence emissivity, of WCs and overlying spray. Their qualitative effects were first investigated by performing small domain SURFER runs with either a continuous foam layer overlying, or

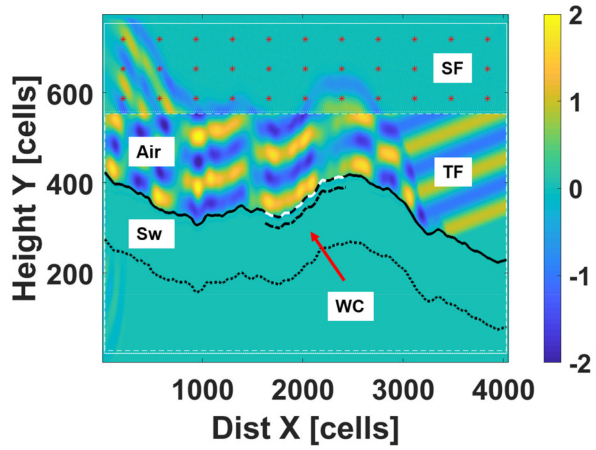

Fig. 3. SURFER *Ez* field plot for a model run with 8-m-wide rough sea surface and 1.6-m-wide 5-cm-thick WC (20% cover) embedded in ambient seawater, Sw. Cell size $dx = 2$ mm. A plane wave propagates down and to right at incident angle 5° off vertical. At this early iteration (1165), the wave approaches the right boundary, while surface reflections in the TF layer start crossing the TFSF boundary into the SF region. (a) Sw: top (solid black) bottom (dotted). (b) WC: top (dashed, white) bottom (dash-dot).

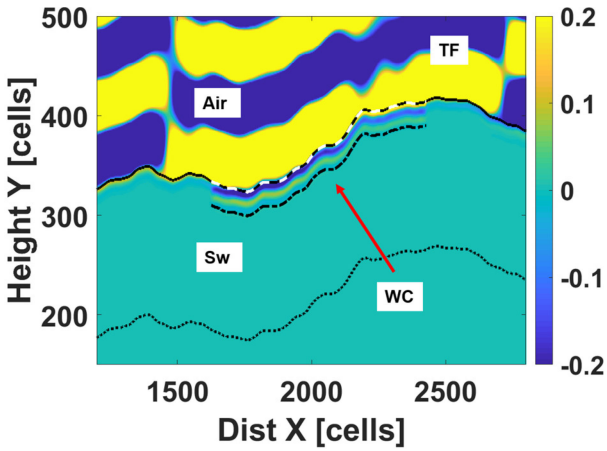

Fig. 4. Close up view of *Ez* in Fig. 3 showing deeper penetration into the WC foam layer (red arrow) than into ambient seawater, Sw. Top and bottom boundaries, respectively, of the foam layer and the Sw are highlighted, as in Fig. 3.

foam patches representing WCs embedded in a flat or rough sea surface, with or without an overlaying spray layer. Intermediate run results (see Figs. 3 and 4) give some insight into model operation. At iteration 1165 (see Fig. 3), the incident plane wave has propagated downward, almost reaching the absorbing PML right model boundary (solid white line). Waves scattered from the rough sea surface and WC are interfering with the incident field in the total field (TF) region, and the reflections, but not the incident wave component, are passing through the TFSF virtual boundary (dashed white), into the SF region, where they are probed and recorded for BRCS and emissivity analysis. At the TFSF boundary, the incident field is simultaneously injected downward into the TF region, and removed, numerically, as it moves upward, into the SF region. This allows the SF to be isolated and probed.

A close-up view of the fields around the WC (see Fig. 4) shows the greater penetration of EM radiation into the WC foam layer than into ambient seawater (Sw). It appears the penetration depth depends on both the local phase and the angle of the incident wave relative to the rough surface. This observation motivates a closer study of the emissivity effects of different combinations of roughness, WCs, and foam (see Section III-A), and consideration of their mutual interactions (see Section III-B).

The quantitative effects of WCs on emissivity of a wind-roughened sea surface were then determined using ensembles of runs with a larger domain, spanning different realizations of the rough surface gravity wave spectrum [7] and randomly distributed embedded WCs parameterized for various wind speeds up to tropical storm force (see Section III-C).

The effects of an overlying spray layer under wind conditions representing a Category 1 hurricane were then considered with the incorporation of the new RTM spray model [26] dielectric profile into the FDTD model to study the WC detectability under such conditions (see Section III-D).

The effects of wave shape and breaking on emissivity were studied next by modeling laboratory nonlinear, asymmetric, and breaking waves, observed in the OHMSETT wave tank (see Section III-E). Finally, the emissivity influence of the synthesized waveforms of different shapes, but with MSS comparable with the lab data, was simulated to determine the secondary effect of sea state, independent of the dominant MSS effect (see Section III-F).

A. Separate Effects of Roughness and WCs

The effect of a rough surface, and additionally, an embedded WC, on the surface emissivity can be determined by statistically comparing runs made with and without roughness and WCs. In Fig. 3, the H-Pol *Ez* field component is shown for a single realization of the rough surface—a short roughness profile generated from the gravity wave spectrum [7] for a wind speed of 5.0 ms^{-1}. The incident plane wave of frequency 1.4 GHz impinges on a single WC of thickness 5 cm and width 1.6 m, at an incident angle of 5° down and to right of nadir. In this and subsequent figures for a rough sea, the *Ez* field component is plotted at a particular model iteration. The effects of the WC in allowing deeper field penetration are clearly evident in the zoomed plot of Fig. 4. However, the diffuse reflections from the rough sea surface obscure those from the WC, the effects of which are barely evident above the surface in the *Ez* plot. The WC emissivity effects are best revealed by an NTFT [23], [24] and BRCS (nondimensional scattering width) analysis, as described in [1]. The resulting ratio of the incident and total power in the far field (normalized BRCS) can be integrated around the unit circle to estimate *r* and hence $e = 1 - r$.

Analysis after completion of the run shown in Figs. 3 and 4, and a companion run made with the same rough surface and forcing, but no WC, showed the WC increased the overall surface emissivity, *e*, from 0.366 to 0.424, an increase of 16% [1]. The model seawater domain with the embedded WC coverage, $W = 20.0\%$, could represent the field of view from a radiometer mounted $\sim$10 m above the surface. However, as shown in Section III-C, expected WC coverage of an extended sea surface for a wind speed of 5.0 ms^{-1} is only 0.1%; thus, the actual and simulated change, for a domain spanning many waves and WCs, is much smaller than for the isolated WC case discussed above.

TABLE I
MEAN OR ACTUAL EMISSIVITIES FOR 36 RUNS WITH VARIOUS ROUGHNESS WCS FOAM AND SPRAY FEATURES

Ens[&] #	FDTD Emiss *e*	Ens Siz	Std Err	WC	Fm	Sp	Rgh
1a	0.3361	1	-	0	0	0	0
1b	0.3878	1	-	1	0	0	0
1c	0.5824	1	-	0	1	0	0
1d	0.9146	1	-	0	0	1	0
1e	0.9109	1	-	1	0	1	0
1f	0.8949	1	-	0	1	1	0
2	0.3662	5	0.0023	0	0	0	1
3	0.4149	5	0.0001	1	0	0	1
4	0.5987	5	0.0014	0	1	0	1
5	0.9156	5	0.0002	0	0	1	1
6	0.9116	5	0.0014	1	0	1	1
7	0.8963	5	0.0003	0	1	1	1

[&]Single model (1a-1f) or ensemble number (2–7) with ensemble size (N = 5). Hyphen (-) indicates not simulated. Feature presence or absence denoted by 1 or 0, respectively. Single model *e* values for flat sea runs are considered exact, while the means are based on 5 rough surface realizations per ensemble and are subject to statistical variation. Hyphen (-) indicates not applicable.

Low *W* values associated with weak winds demands high sensitivity from both the simulations and from the actual radiometers flying at aircraft or satellite altitudes. For example, the *C*-band stepped frequency microwave radiometer, flown on the NOAA hurricane hunter, which responds mainly to the presence of WCs, can only resolve wind speeds at $< 10\%$ error down to about 10 ms^{-1} [33]. *L*-band radiometers are even less sensitive when retrieving winds in low *W* conditions.

B. Combined Effects of Roughness, WCs, and Spray

To investigate the combined effects of roughness, WCs, and also overlying spray, a six-member series of runs, based on that of Fig. 3, was executed with a flat sea plus MC ensembles of five different roughness realizations of the gravity wave spectrum [7] at 5 ms^{-1} wind speed (36 runs in total). The series represents seawater with or without the 5-cm WC, or continous 5-cm-thick foam, optionally overlain by a 5-cm spray layer. The results are given in Table I, which gives the overall emissivity and std error and shows the oceanographic features, i.e., WC, continous foam cover, Fm, and or spray, Sp and surface roughness, Rgh, that are present in each run (if the corresponding table entry is unity). For the flat sea runs (1a-1f), *e* is considered exact and no std error is given, since there were no random roughness realizations. Differencing *e* between models in pairs (see Table II) gave an incremental roughness effect of 0.030 and respective WC, foam, and spray effects of 0.052 (0.049), 0.246 (0.232), and 0.578 (0.549) for a flat (rough) sea. In addition to

TABLE II
EFFECTS OF ROUGHNESS WCS FOAM AND SPRAY DIFFERENCES

Pair No.	Ens[&] Pair #-#	Stud. t 3.355 or 4.604 (99%)	Std Err Mean Diff.	Emiss *e* Diff.	Diff. Features	Comm. Features
1	2-1a	13.289	0.0023	0.0301	Rgh	None.
2	3-1b	9.636	0.0028	0.0270	Rgh	WC
3	4-1c	11.872	0.0014	0.0163	Rgh	Fm
4	5-1d	14.098	0.0001	0.0010	Rgh	Sp
5	6-1e	3.679	0.0002[#]	0.0007	Rgh	WC+Sp
6	7-1f	5.507	0.0003	0.0014	Rgh	Fm+Sp
7	1b-1a	NA	NA	0.0517	WC	Flt
8	3-2	13.52	0.0036	0.0487	WC	Rgh
9	1c-1a	NA	NA	0.2463	Fm	Flt
10	4-2	87.78	0.0027	0.2325	Fm	Rgh
11	1d-1a	NA	NA	0.5785	Sp	Flt
12	5-2	242.42	0.0023	0.5494	Sp	Rgh
13	1e-1a	NA	NA	0.5748	WC+Sp	Flt
14	6-2	239.92	0.0027	0.5454	WC+Sp	Rgh
15	1f-1a	NA	NA	0.5588	Fm+Sp	Flt
16	7-2	232.56	0.0023	0.5301	Fm+Sp	Rgh
17	1f-1d	NA	NA	-0.0197	Fm	Flt+Sp
18	7-5	73.127	0.0003	-0.0193	Fm	Rgh+Sp
19	1f-1c	NA	NA	0.3125	Sp	Flt+Fm
20	7-4	13.822	0.0014	-0.0193	Fm or WC	Rgh+Sp
21	1e-1d	NA	NA	-0.0037	WC	Flt+Sp
22	6-5	19.700	0.0002	-0.0040	WC	Rgh+Sp
23	1e-1b	NA	NA	0.5231	Sp	Flt+WC
24	6-3	176.85	0.0028	0.4967	Sp	Rgh+WC

[&]Runs or ensembles differenced are those appearing in Table I. [#]Emissivity statistically significant at 95% level; all others at 99% level. Single model (1a–1f) or ensemble number (2–7) with ensemble size ($N = 5$). NA indicates not applicable. For runs 1a–1f there is no roughness variation, so *e* is considered exact. Student t critical values are 3.355 (8 dof) or 4.604 (4 dof, Pairs 1–6) at 99% significance level.

the emissivity differences and their statistical properties, the table tabulates the features that were common to both members of the pair (last column) and those that were different (column 6). In pairs including flat sea runs, only the rough one of the pair contributes to the std error. For all pairs that included one or two five-run ensembles (involving rough surface variation), differences were statistically significant at the 99% level, with the exception of pair 5 which was significant at 95%. The significance levels were determined by performing t-tests using the mean difference of each pair and corresponding std errors, with the numbers of degrees of freedom (dof), given in the Table II caption.

Noticeable interactions among the effects of the various features occurred, with a tendency for mutual reductions in *e* effect, when multiple features were present. Note the progressive reduction of roughness effect with the addition of WC, Fm, and Sp or combinations of these (pairs 1–6). For example, the effect of roughness (compared with a flat sea run) when a WC was present was much reduced when spray was also present (compare pairs 2 and 5), although the effect was less dramatic when there was continous foam cover in place of a WC (pairs 2 and 6). Also, the effects of WC and Sp (pairs 13 and 14) or of Fm and Sp (Pairs 15 and 16) were quite different for the flat sea and rough sea cases,

TABLE III
KEY FDTD MODEL PARAMETERS FOR RUN AT 12 ms^{-1} WIND SPEED WITH WHITECAPS (AS SHOWN IN Fig. 5)

Parameter	Value	Unit	Remark
Number of WCs	3	-	Depends on *s* and *W*
WC Mean scale (*s*)	3.9	m	$s=0.60*U_{10}^{0.75}$,Gamma pdf
WC Coverage (*W*)	2.2	%	$W=2*U_{10}^{3.75}x10^{-6}$ [27, 28]
X,Y- Domain size	256.0, 1.5	m	Excludes PML
Water layer depth	25	cm	Conforms to surface
Foam thickness	5	cm	Conforms to surface
Void fraction (*Vf*)	0.01-0.60	-	Largest at surface [10]
Incidence angle	5	deg	Plane wave from top left
Model cell size (*dx*)	5	mm	FDTD spatial resolution

suggesting that roughness is a significant factor influencing the effects of WCs and Fm. Sp evidently has very large impact on the emissivity in almost all cases, regardless of which features are common to both runs (see, pairs 11, 12, 19, 23, and 24), while if Sp is present, the other features, e.g., Fm, or WC have little effect (pairs 17, 18, 20, 21, and 22). The dominant effect of spray on emissivity likely arises from vertical variations in *Vf* and associated dielectric constant profiles. These provide effective impedance matching between pure air and seawater [10], [26] which reduces the reflection intensity. In some instances, we see evidence that an intervening Fm layer (or large WC) can also improve the impedance match (pairs 4 and 5). However, the effect of Sp is apparently greater for a flat than for a rough sea, if a WC is present (contrast pairs 23 and 24). These effects might be better understood through an analysis of the radiative transfer processes occuring in the dielectric layers, consistent with energy conservation (implied by *Kirchhoff's* law $e + r = 1$), while recognising that the actual geometrical shape of the dielectric surfaces also plays a significant role, by changing the local angle of incidence on surface wave facets.

While we have shown feature effects for just one set of WC, Fm, and Sp parameters and only one wind speed, the results strongly suggest there are nonlinear interactions among the various oceanographic features influencing emissivity. Thus, significant errors can arise with the common practice in emissivity modeling of assuming such effects are independent and additive. This is particularly the case, for the combined emissivity effects of roughness and foam patches associated with wind-dependent WC cover, which we address quantitatively in Section III-C.

C. Emissivity of Wind-Dependent WC Cover

Repeated SURFER 2D runs spanning a larger 256-m-wide domain were made, with one calm and three to nine rough surfaces representing independent realizations of the work presented in [7] at each of seven wind speeds (U10 = 5, 7, 8, 10, 12, 15, and 20 ms^{-1}), with and without continuous foam cover, or embedded WCs. For instance, the H-Pol *Ez* field for 12 ms^{-1} (see Fig. 5) was generated using the parameters given in Table III.

Wind speed dependent empirical formulas for WC mean scale (*s*) [27, Tropical Zone: eq. (6)] and fractional coverage (*W*) [28, eq. (3)] were used to determine the number and mean size of WCs required for each run. These generally increased as wind

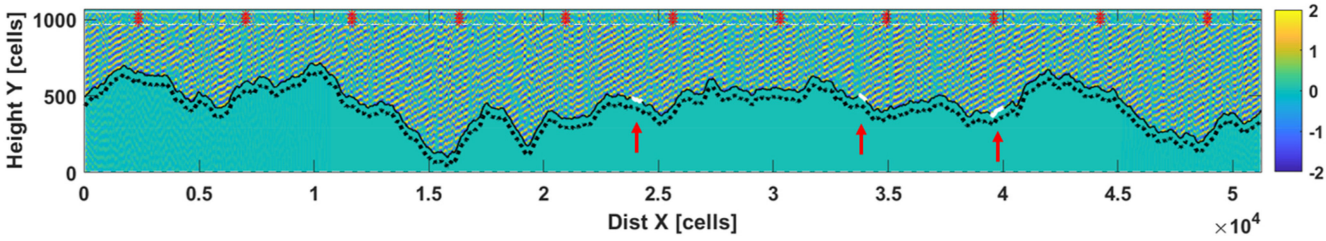

Fig. 5. Simulation of Ez field for wind-roughened sea surface ($T = 20$ °C, $S = 34$ psu) showing three embedded WCs (white lines at arrows) randomly positioned in a 256-m-wide domain, and of a scale and coverage statistically selected for a wind speed of 12 ms^{-1}. (See text and Table III, for surface and WC parameters.)

TABLE IV
FDTD EMISSIVITY MEAN AND STD ERROR FOR ENSEMBLE WC RUNS AT EACH WIND SPEED, U_{10}

U_{10} (ms^{-1})	No WCs	Mean WC Scale s (m)	WC Cover W (%)	FDTD Overall Surface Mean(e)	Ref. Model[&] Overall Surface e	FDTD Rough Effect Mean(e)	FDTD WC Effect Mean(e)	FDTD Overall Surface Ster(e)	FDTD Rough Effect Ster(e)	FDTD WC Effect Ster(e)
0.0	0	NA	NA	0.30729(1)[#]	0.31505	NA	NA	NA	NA	NA
5.0	1	2.0	0.1	0.33391(9)	0.31814	0.03965(9)	0.00218(9)	0.00192	0.00059	0.00207
7.0	1	2.6	0.3	0.33867(9)	0.31954	0.04750(9)	-0.00277(9)	0.00051	0.00269	0.00232
8.0	2	2.9	0.5	0.34255(9)	0.32081	0.03472(9)	0.00054(9)	0.00284	0.00234	0.00325
10.0	2	3.4	1.1	0.35269(6)	0.32505	0.04925(6)	0.00193(6)	0.00377	0.00263	0.00250
12.0	3	3.9	2.2	0.36033(3)	0.32957	0.03934(3)	0.01370(3)	0.00871	0.00033	0.00839
15.0	4	4.6	5.2	0.38230(3)	0.33930	0.05064(3)	0.02437(3)	0.00568	0.00943	0.01510
20.0	8-13	5.7	15.1	0.39236(3)	0.36555	0.05213(3)	0.03294(3)	0.00101	0.00479	0.00486

[&]Model: Klein and Swift [25], SSA/SPM [31]–[33]. [#]Ensemble size (N), where $N = 1$–9. NA indicates not applicable.

speed increased. Model vertical domain size was also increased to accommodate higher waves. The number of WCs and the values and formulas for U_{10}-dependent s and W are given in Table III. The remaining parameters given in this table were the same for each run.

Sufficient numbers of WCs (1–13) of various sizes, s, were sampled from a Gamma probability density function (pdf) [27] to account for specified coverage, W, and the sample was distributed across the surface, using a uniform pdf. This distribution could represent passive foam patches persisting for several wave periods after breaking events. In contrast, active foam associated immediately with breaking would tend to occur at wave crests, as described in Section III-E.

Results from a statistical analysis of the multirun ensembles are given in Table IV, with selected columns (5–8) plotted in Fig. 6, along with their 95% confidence limits. Comparisons between flat sea, roughness, and WC runs revealed the mean overall effect on surface emissivity, and mean contributions of roughness and foam patches (WCs) of varying size, but identical thickness and void fraction range.

Results are compared with predictions from reference emissivity models for contributions of the flat sea e=0.315 for given T and S [25], roughness (SSA/SPM, [29], [30]), and foam [31] to overall sea surface emissivity (see, col 6, Table IV). The mean deviation of total e between the FDTD and semianalytical reference model predictions was 0.026 +/- 0.006, with FDTD higher by about 8%. For each wind speed and roughness realization,

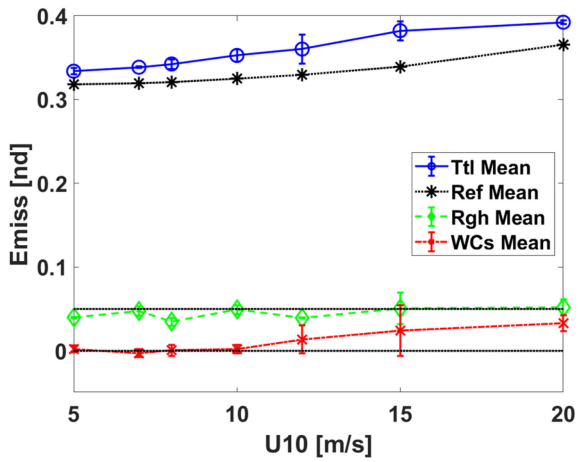

Fig. 6. FDTD and reference model overall surface mean emissivity and roughness and WC effects versus wind speed for multiple runs (plotted from Table IV, cols 5–8). The 95% confidence intervals (two times standard error) and guidelines at Ems values of 0.0 and 0.05 are also shown.

the emissivities from a run with surface only, and one with WCs embedded in the same surface were differenced to determine the enhancement effects of the WCs. Similarly, the emissivity for the flat sea case ($U_{10} = 0$) was subtracted from that of each roughness case (without WCs) to estimate the roughness effect. As expected, the overall (total) e, which includes both these

effects, increased monotonically with increasing wind speed. The roughness and WC effect, considered in isolation, also tended to increase with increasing wind speed.

Comparing the means and their standard errors for each ensemble and emissivity effect shows the roughness increase (see, col 7, Table IV) was statistically significant at the 95% probability level (determined by 1.96 times the std error), at all wind speeds, while the WC effect (col 8) was significant at 65% level in most cases, but at the 95% level at 20 ms^{-1}. As illustrated in Fig. 6, both effects increased monotonically at speeds above 10 ms^{-1}. The WC effects are either not significant or marginally significant at slower speeds, and the negative value for 7 ms^{-1} is likely unphysical. This is not surprising since at such low speeds W $\sim$ 1% or less and WCs are small and rarely observed, so the model (and most radiometers) are at or below their WC detection limits.

It is remarkable that the increase in WC effect with wind speed above 10 ms^{-1} is clearly evident, while the trend of the roughness effect appears marginal. This could be due to the removal of the dominant linear effect of roughness on WC effect by the differencing, in pairs, of runs with the same rough surface. The residual variations among pairs having different rough surfaces might then be explained by the nonlinear effects of roughness on WC effect, described in Section III-B. The results at higher wind speeds could be considered conservative, since a constant foam thickness and void fraction range were used (see Table III). If these parameters are larger under actual storm wind conditions, as illustrated in Section III-D, the trend of the WC effect could be stronger.

The statistical accuracy and precision of the FDTD model at any wind speed can be improved by using smaller grid cells (reducing numerical dispersion), and by running additional MC simulations (increasing statistical power), which require additional memory and run time. We attempted to simulate roughness and WC effects at higher wind speeds (up to 35 ms^{-1}, representing a category 1 hurricane). However, the expanded domain required to accommodate the larger and longer dominant waves demanded excessive run times on the available workstation (18 days for the largest 35 ms^{-1} model!), even after doubling the FDTD cell size from 5 mm to 1 cm. While technically within the usual factor of 20, used to minimize FDTD numerical dispersion, that cell size nevertheless produced e values of questionable accuracy. More advanced parallel architectures or super computing equipment will be needed to address this issue. (Our GPU could not operate on these large domains, due to memory constraints and limitations of the available software.)

D. Spray Effect in Hurricane Winds

The spray layer employed in Section III-C (henceforth, Sp1) was adapted from the foam layer RTM model [10] with specified thickness and void fraction profile shape and range. A more realistic model, designed specifically to simulate sea spray, for which the layer thickness is assumed to be proportional to the significant wave height (Hs) has recently been developed [26]. In contrast to Sp1, which has an exponential void fraction profile [10], the new model, Sp2, has a power law profile [26]. Both models employ the same refractive mixing rule to determine the combined dielectric properties of the air and water fractions comprising the spray.

TABLE V
FDTD AND RTM EMISSIVITY FOR CAT. 1 HURRICANE

Run[&] #	FDTD Emiss e	No. WCs	WC Thick-Ness (m)	Spray Model Sp1/2	Spray Thick-Ness (m)	Surface Type
6	0.16387	0	NA	NA	NA	Flat
5	0.95450	0	NA	Sp2	24.15	Flat
1	0.94166	1	0.05	Sp2	24.15	Rough
7	0.94077	1	0.30	Sp2	24.15	Rough
2	0.98241	1	0.30	Sp1	0.50	Rough
3	0.33455	1	0.30	NA	NA	Rough
4	0.94134	0	NA	Sp2	24.15	Rough

[&] Parameters for all runs: U_{10} =35 ms^{-1}, Hs = 8.05 m, S = 34.0 psu, T = 20°, inc. angle= 5°, frequency= 1.413 GHz, for Sp2: thickness = 3Hs. For FDTD: WC scale s=8.6 m, void fractions Vf=0.01–0.60 (WC), 0.6–0.97 (Sp1), 0.5–0.99 (Sp2). NA indicates not applicable.

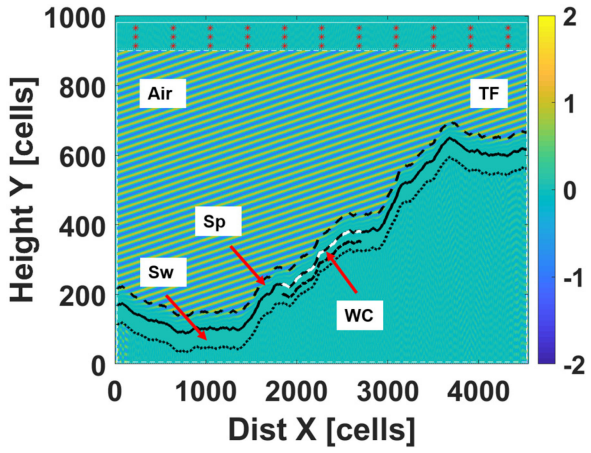

Fig. 7. *Ez* fields showing plane wave incident on a 1.6 m diameter WC of 30 cm thickness (top white solid, line, bottom blue dashed), centered in a 9-m-wide domain, and overlaid by a 50-cm-thick spray layer, Sp1 (top red dashed), overlying the WC and Sw (green, dashed line). dx = 2 mm.

Seven SURFER 2D model runs were made with different surface features including presence and thickness of a WC and spray layer and a flat or rough sea surface (see Table V). An example of one of the runs is shown in Fig. 7. These runs were used to compare the results from the two spray models, and to study the effect of a spray layer on WC detectability under wind and wave conditions representative of a category 1 hurricane. A relatively short model sea surface domain of width 9 m was used, with a roughness and significant wave height, Hs = 8.0 m, obtained from the wave spectrum [7] for a wind speed of 35 ms^{-1}. In the example, the WC and spray layer thicknesses were 0.30 and 0.50 m, respectively. For the Sp2 model runs, the spray layer thickness was 24.00 m, consistent with the wind speed and Hs [26].

TABLE VI
FDTD CAT. 1 HURRICANE RUN DIFFERENCES

Run[&] Pair #-#	Emiss *e* Diff.	Different Feature	Common Feature	Effect
5-6	0.7906	Sp2	Flat Sea, No WC	Sp2 on flat sea
7-3	0.6062	Sp2	Rough,Thck WC	Sp2 on rough sea
2-3	0.6479	Sp1	Rough,Thck. WC	Sp1 on rough sea
2-7	0.0416	Sp Mdl	Rough,Thck WC	Sp1 v's Sp2
7-4	-0.0006	WC	Rough Sea, Sp2	Thick WC
1-4	0.0003	Thn WC	Rough, Sp2	Thin WC
7-1	-0.0009	Thk-Thn WC	Rough, Sp2	Thick v's thin WC
4-5	-0.0132	Rough	Sp2, No WC	Rough sea under spray

[&] Runs differenced are those appearing in Table V.

The predicted emissivities for the runs (see Table V) and *e* differences between selected pairs (seeTable VI) can be used to determine the effects of the WC, spray layer, and surface roughness. The emissivity value of 0.955 for the SURFER 2D flat sea case (run 5), which includes both the Sp2 spray layer and flat sea contributions, compares closely with the value of 0.986 obtained from the new 1-D RTM spray model [26], from which the SURFER 2D spray void fraction profile was obtained. The difference of 0.031 represents a departure of just 3.2%, which, considering the different model physics and dimensionality, shows remarkably close agreement.

The remaining pairwise comparisons reveal some interesting effects: Emissivity differences for pairs 5–6, 7–3, and 2–3 show that the spray enhances *e* (and hence reduces *r*) dramatically; more so over, a flat than a rough sea with a WC. Spray layer Sp1, thinner than Sp2 by a factor of 48, and with a slightly narrower *Vf* range has a comparable, but slightly larger *e* effect (see footnote, Table V for *Vf* and other parameters used in RTM and SURFER 2D).

The Sp1 simulation (see Fig. 7) shows the incident plane wave strongly attenuated in the foam layer with consequently no significant scattering in the overlying TF and SF regions (with probes marked by asterisks) of the domain. A similar effect was observed with the much thicker Sp2 model runs. Contrast this with the strong interference pattern produced by the incident and SFs in FDTD field plots for runs without a spray layer (e.g., Figs. 3 and 5). Interestingly, Anguelova and Geiser [10] found that *Vf* at the top of a foam layer had a more important influence on the emissivity response than did layer thickness. This has a practical implication for FDTD modeling, since the Sp2 layer, of thickness 3–5 times *Hs*, demands a larger computational domain and cost. This cost can be lowered if use of a thinner spray layer model (e.g., Sp1, see Fig. 7) can be justified in terms of an equivalent attenuation effect.

Pairs 7–4, 1–4, and 7–1 show that the Sp2 spray layer obscures the sea surface to the extent that differences in WC thickness, and indeed the effect of the WC itself, are insignificant. This suggests that radiometric detection of WCs under the storm conditions specified in the model would be unlikely, given the precision limitations of available ocean remote sensing radiometers.

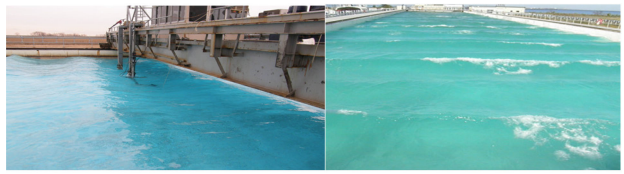

Fig. 8. OHMSETT tank with WNL (left, showing instrument bridge) and SNL breaking waves (right, viewing front face) [13].

The preliminary results shown here demonstrate both the relative accuracy of the RTM and SURFER 2D spray layer implementations, and their potential applications in studies of microwave radiometer and reflectometer responses under tropical storm and hurricane conditions. Anticipating further advances in observing storm wind and wave fields *in situ*, and associated WC, foam, and spray properties, SURFER sensitivity tests could be employed to predict *e* and *r* for comparison with radiometer and reflectometer retrievals, as an aid to enhance understanding of factors influencing *L*-band remote sensor performance.

E. Wave Asymmetry and Breaking

SURFER runs were also made based on a quasi-periodic train of nonbreaking weakly nonlinear (WNL), and breaking strongly nonlinear (SNL), water waves (see Fig. 8) generated in the OHMSETT wave tank [34]. The WNL waves exhibited horizontal asymmetry due to instability in the wave generation process, but no breaking. In the simulation, these waves were illuminated by a 1.413 GHz plane wave incident at +/− 37.5° [see Fig. 9(a) and (b)]. Variation of *Ez* intensity above each individual waves is evident in the TF and SF regions above the surface. The BRCS plots (c)(e) and their difference (f), with angular scales for the -37.5° incidence BRCS (e) reversed in (d) and in the input to (f) for ease of interpretation, reveal how asymmetry of nonbreaking waves affects emissivity. Here, the asymmetry due to crest flattening on the forward face produces a dual-beam forward scatter response [see Fig. 9(a)]. In the ocean, this effect could manifest as an EM response to upwind/downwind asymmetry of the wind-wave field. The asymmetry shown in the figure produces, approximately, a 12% change in *e* when the two cases (+/- 37.5°) are compared with each other.

Unlike WNL waves, the SNL wave heights [see Fig. 10(a) and (b)] were intentionally modulated by beating effects due to small variations in wave paddle period [34]. They were also steeper, to the point of breaking and displayed more vertical, but less horizontal, asymmetry. WCs formed, as seen in photographs (e.g., right panel, Fig. 8) and their scale and location were inferred from measurement thresholds of local steepness and shear velocity. Mean WC thickness, based on photos (not measured *in situ*), was set to 5 cm.

In contrast to the WNL case, which exhibited forward scatter [see beam orientation in Fig. 9(c)], the SNL waves are sufficiently steep to cause backscatter at the specified +/−37.5° incidence angles [see Fig. 10(c) and (d)]. In this case, the wave

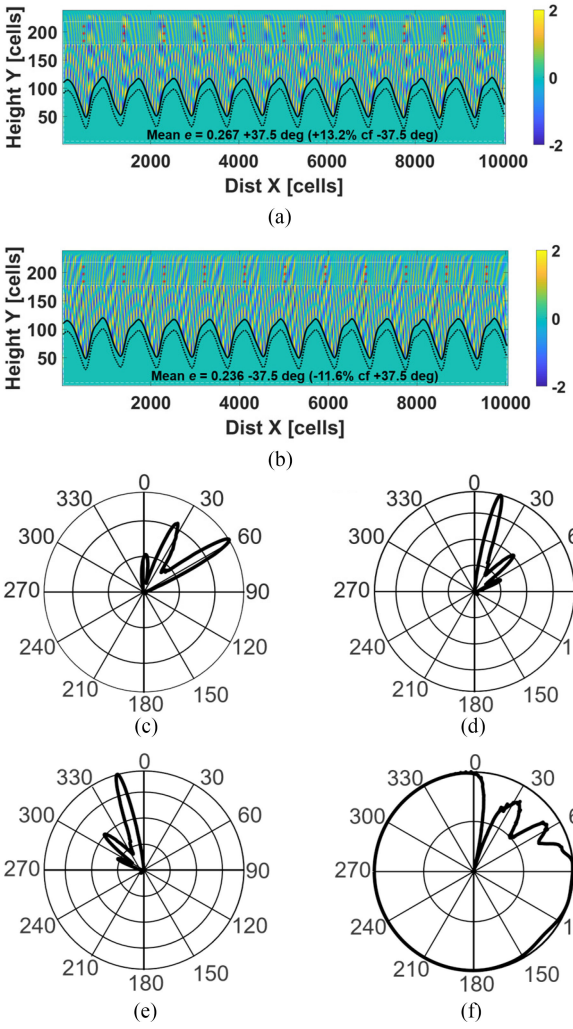

Fig. 9. Effect of weakly NL waves on emissivity of waves in the OHMSETT tank. Forward scatter dominates the *Ez* response. Cell size, $dx = 5$ mm and domain width is 50 m. Incidence angle +/- 37.5° for (a) and (b), respectively, with corresponding BRCS plots in (c) and (e). The BRCS difference, computed with angular scale of (e) reversed as in (d) is shown in (f). BRCS plot scale is nondimensional (nd) linear factor with interval of 500, or 1000 for (f). (See text for other details.)

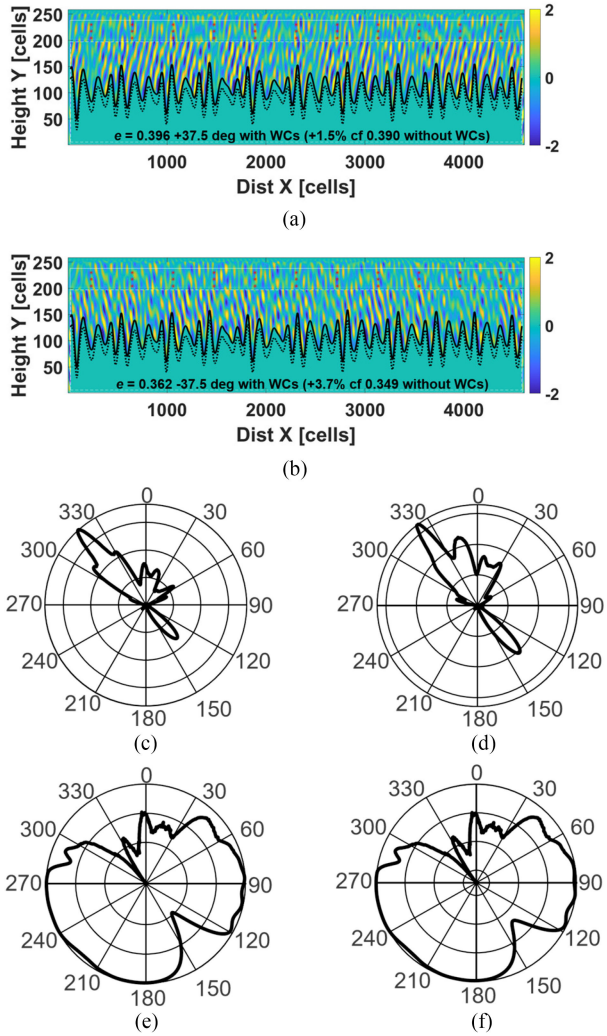

Fig. 10. Effect of strongly NL waves on emissivity of breaking waves in the OHMSETT tank. Back scatter dominates the *Ez* response. $dx = 5$ mm and domain width is 50 m. Incidence angle +/- 37.5° for (a) and (b), respectively with corresponding BRCS plots in (c) and (e). Corresponding BRCS difference plots (e) and (f), after angular scale reversed in (d) reveal wave asymmetry effects both in the presence (e) and absence of WCs (f). Only the non-WC *Ez*, plots not shown. BRCS plot scale is nd linear factor with interval of 100. (See text for other details.)

groups produced by paddle-induced modulation (indicated by periodic occurrence of higher waves) cause corresponding variations in *Ez* intensity [see Fig. 10(a) and (b)]. The BRCS plots (c) and (d) and BRCS difference plots (e) and (f), with angular scales reversed in the −37.5° incidence cases) reveal some wave asymmetry effects both in the presence (c)–(e) and absence of WCs [(f), non-WC *Ez* plots are not shown]. However, the figures show *e* changes of only 1%–3% between +/-37.5° incidence for the WC and no-WC cases. The asymmetry of *e* is mild because the SNL waves, though steep and high, have a more horozontally symmetric form than the WNL waves. The similarity of BRCS difference plots (e), (f) indicates that the WCs have little impact on the asymmetry of the *e* response, which is dominated by differences in backscatter from the forward and back wave faces. In contrast to the randomly distributed waves and "passive" WCs of Fig. 5 that could represent persistent foam patches formed by previous breaking events, the more regular waves of Fig. 10, with WCs appearing at or near the breaking wave crests, indicate the likely effect on emissivity of more active WCs, representing transient foam patches formed by currently evolving breaking events.

F. Effect of Waveform

To investigate the combined effect of waveform and incidence angle on *e*, waveforms of sinusoidal (Sin), second-order stokes (St2), and random waves (Kud, generated from [7]) were synthesized to match the SNL (lab) waves generated in the OHMSETT tank (see Fig. 11), in terms of the resulting MSS. The synthesized waveforms were chosen to represent low swell (Sin), nonlinear waves with flat crests and sharp troughs (St2)—a shape that, in deep water, is thought to produce the so-called EM

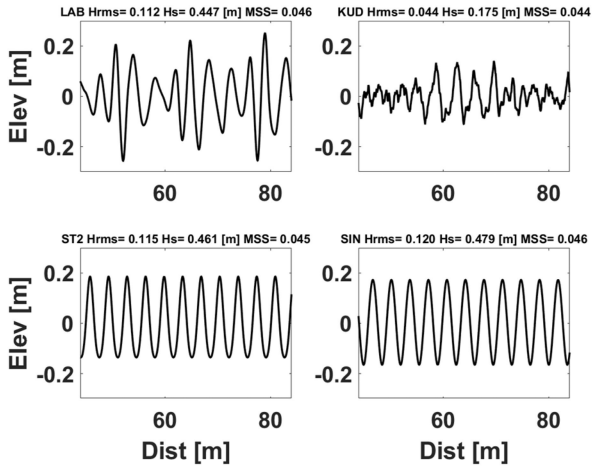

Fig. 11. Elevation (m) of lab and synthesized waveforms with the same nominal MSS. Values of the RMS and significant wave height, and of mean square slope, are shown above each plot.

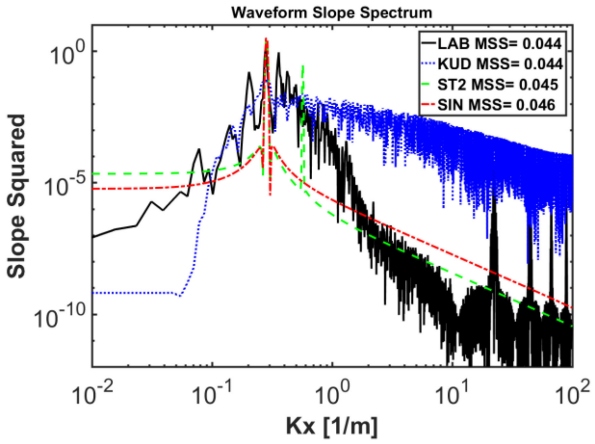

Fig. 12. Slope spectra of wave tank and synthesized waveforms for the 127-m domain used in the FDTD runs. MSS values are shown in the legend.

bias in radar altimetry, and which can be exagerated in shallow water, and a random wind sea (Kud). The waveform spatial series (see Fig. 11) and their wavenumber (Kx) spectra (see Fig. 12) show that the bandwidth progressively increases from the monochromatic Sin case, through St2, with its second harmonic and vertical asymmetry, through the lab waveform and the broader banded, but less energetic random, Kud, case, with wave slopes concentrated at higher wavenumbers.

The SNL lab data in this case were corrected for the effects of Doppler shift and transformed to the spatial domain using the relative motion of the sensor bridge and the phase speed of the dominant gravity wave, based on the deep water dispersion relation. This contrasts with the approach used in the previous section for the SNL case, in which only the sensor bridge speed of 0.53 ms^{-1} was used, assuming the waves were "frozen" in space. That made the wavelengths appear much shorter in the SURFER 2D model domain than they were in the tank. In contrast, the WNL data, sampled from a stationary bridge, were transformed to the spatial domain using the deep water dispersion relation, producing waves of realistic length [compare Figs. 9(a) and 10(a)]. For this section, using the relative motion of the sensor bridge (0.53 ms^{-1}) and the waves (phase speed 2.34 ms^{-1} based on the wave paddle period of 1.5 s and the dispersion relation), as they advanced toward one another, a more realistic SNL spatial waveform with dominant wavelengths of approximately 4 m (see top left panel, Fig. 11) was obtained. While the deep water wave relation was accurate enough for the purpose of producing a realistic waveform, the waves, strictly speaking, were marginally transitional, with water depth approximately one quarter of the wavelength.

The more idealized nonlinear and random waveforms were also synthesised to match the dominant wavenumber of the spatially transformed lab SNL waveform and their height was adjusted to match their MSS with the value of 0.0446 computed from that waveform. Since *L*-band microwave reflectometers and radiometers primarily respond to the effects of MSS (or BRCS), this approach allows the secondary influence of waveform (also described by elevation spectrum or "sea state") to be assessed. The simulated random "wind-wave" case (Kud) was generated using the spectrum [7] with the same dominant wavenumber as the spatial lab waveform (equivalent to a wind speed, $U_{10} = 8.52$ ms^{-1}). In this case, a very young inverse wave age value of 3.64 (4.4 times higher than the value of 0.83 for a fully developed sea) was needed in the spectral model to match the lab waveform MSS. This concentrates the wave slopes at higher wave numbers in comparison with the narrow banded waveforms centered near the peak wavenumber. It also produces a spectrum with a significantly lower signficant wave height *Hs* of 0.175 m for Kud compared with about 0.460 m for the other waveforms.

For simplicity, given the relatively light "equivalent" wind and, correspondingly, low predicted WC cover, the existence of WC's associated with breakers observed in the laboratory wave data, and modeled in Section III-E, was ignored in these runs (i.e., no foam patches were embedded in the observed lab or simulated rough surfaces). The emissivity values predicted by FDTD (see Fig. 13) show significant variation, and also differences in mean value (see legend), across incidence angle, resulting from interactions of the EM plane wave with the linear (Sin), nonlinear (lab, St2), or random (Kud) geometry of the underlying sea surfaces.

The pattern of *e* variation for the Sin and St2 waveforms, which, as expected for H-pol, is typically decreasing with increasing incidence angle, is similar to that of the lab waveforms; almost identical at nadir (incidence angle 0°, corresponding to minimal backscatter for a downward looking radar), but decreasing more slowly with increasing angle. In contrast, the random Kud waveform produces significantly lower *e* values at all but the highest incidence angle (49°), where it falls between the Sin and St2 case.

This *e* pattern could be due to roughness, or equivalently steeper slopes, being concentrated at higher wavenumbers, and to the relatively low rms wave height, Hrms = 0.175 m, of waveform Kud, compared with values of 0.478, 0.461, and

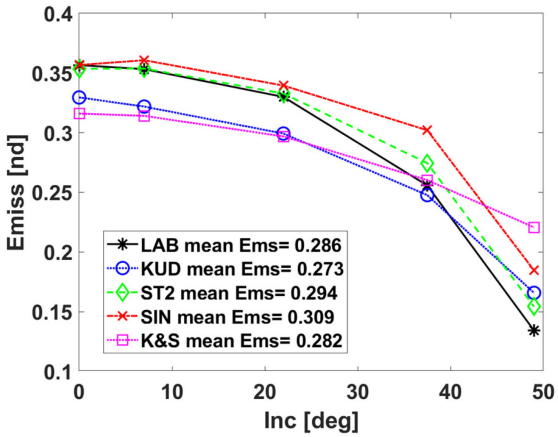

Fig. 13. Emissivity versus incidence angle for laboratory and synthesized waveforms used in the FDTD runs. The predicted flat sea emissivity response from [25] is overlaid (solid magenta line with square markers).

0.447 m for the narrower banded Sin, St2, and Lab waveforms, respectively. Note that the corresponding MSS values (see plot titles, Fig. 11) are nearly the same—the Kud case deviates slightly because the waveform represents only one statistical realization of the spectrum for which the MSS was specified. Comparison with the flat sea response in [25] suggests the random, Kud, waveform with slopes concentrated at high wavenumber and a low *Hs* value, when viewed from nadir, resembles a flat sea more than do the narrow-banded Sin, St2, and lab waveforms, which have a higher *e* and lower *r* at low observation angles.

IV. Conclusion

SURFER 2D was used to model WCs embedded in calm and wind-roughened sea surfaces specified using a realistic wave spectrum model and empirical formulas for WC coverage and scale. The statistically significant results show the expected increase in roughness and WC emissivity effect with increasing wind speed (up to tropical storm wind speeds of 20 ms^{-1}), as predicted by semianalytical sea surface emissivity models. However, those models assume that the roughness and foam (WC) effects vary independently and add linearly, while results from the FDTD model run suggest that the effects of WCs could be modified by the associated surface roughness (i.e., the foam and roughness effects are coupled by WC shape). WNL and SNL (breaking) waves generated in a large wave tank were investigated to determine the effects of observed horizontal and vertical asymmetries, and of the associated WCs on emissivity, and the FDTD model was found to be sensitive to these effects. In contrast to the semianalytical emissivity models, the FDTD model easily accounts for such roughness effects as WC edge diffraction, multiple reflections, and wave shadowing, which are difficult to model analytically.

In addition to the effects of wind speed, which increases the MSS, we also investigated the *e* and *r* response to differently shaped surfaces exhibiting the same MSS as the SNL tank-generated waves. Comparisons were made between the *r* and *e* response to the observed tank-generated waves and synthesized elevation profiles of linear (sinusoidal), nonlinear (Stokes), and fully random (Kudryavtsev distributed) waveforms over the same horizontal domain, as a function of incidence angle. In theory, the MSS should fully determine the roughness emissivity effect. However, it was found that variations in waveform significantly affected the incidence angle dependence of *e* for surfaces having the same MSS. In the fully random case, the observed MSS value was consistent with a young random sea (with inverse wave age 4.4 times that of a fully arisen sea), at a wind speed of 8.5 ms^{-1}. As expected from wave growth theory, and confirmed by our SURFER 2D runs at multiple wind speeds, a fully arisen sea at such a wind speed, with [7] parameterized accordingly, has a much larger dominant period, *Hs* and MSS, and it produces a significantly stronger emissivity effect.

This finding of an *e*, and hence *r*, dependence on wave age for seas of a given MSS accords with recent findings of the CYGNSS mission team. In order to obtain accurate wind retrievals, they found it necessary, at least as an interim measure, to develop two separate retrieval algorithms, one for young seas characteristic of tropical storms and hurricanes and another for fully arisen seas characteristic of large-scale synoptic wind fields, absent major storms [4].

In SURFER 2D, we have implemented well-established and tested state-of-the-art FDTD algorithms, and have applied them in a novel study of wind-driven, linear, nonlinear, and random sea surfaces, with superimposed foam or WCs and, optionally, overlying spray. The resulting model constitutes an accurate, flexible, and powerful tool for studying the interactions of microwave radiation with rough sea surfaces, with a degree of realism not achieved in previous FDTD studies of sea surface roughness. Future SURFER runs, taking better advantage of parallel computer architectures, are planned to extend the results to higher wind speeds using larger model domains, and to improve the statistical significance of the roughness and WC emissivity predictions using more MC runs per ensemble.

SURFER 2D necessarily assumes simulated gravity waves are propagating downwind in the vertical (*x--y)* plane of incidence, and are of uniform profile and infinite length in the third (*z*) dimension. In this configuration, no scattered energy can arrive from out of plane reflections. SURFER 3D will remove this constraint by taking into account out of plane reflections and emissions, allowing radiative effects of directional spreading of the gravity wave field to be studied.

A parallel research effort to use the MoM EM simulation method as an alternative to SURFER 2D for runs at high wind speeds that are costly using FDTD is also progressing (J. Ouellette, NRL Remote Sensing Division, pers. comm.). More deterministic 2-D and 3-D run configurations to simulate active WCs of various shapes, with differing foam thickness and void fraction, embedded in breaking wave crests of specified form are planned. These will require fewer computational resources than MC simulations of randomly rough surfaces reported here.

REFERENCES

[1] D. M. Burrage, M. D. Anguelova, D. W. Wang, and J. C. Wesson, "Modeling L-band reflection and emission from seawater, foam and whitecaps using the finite-difference time-domain method," *IEEE Geosci. Remote Sens. Lett.*, vol. 16, no. 5, pp. 682–686, May 2019, doi: 10.1109/LGRS.2018.2881159.

[2] N. Reul, J. Tenerelli, B. Chapron, D. Vandemark, Y. Quilfen, and Y. Kerr, "SMOS satellite L-band radiometer: A new capability for ocean surface remote sensing in hurricanes," *J. Geophys. Res.*, vol. 117, no. C2, Feb. 2012, Art. no. C02006, doi: 10.1029/2011JC007474.

[3] T. Meissner, L. Rcciardulli, and F. J. Wentz, "Capability of the SMAP mission to measure ocean surface winds in storms," *Bull. Amer. Meteorol. Soc.*, vol. 98, no. 8, pp. 1660–1677, Aug. 2017, doi: 10.1175/BAMS-D-16-0052.1.

[4] C. S. Ruf, S. Gleason, and D. S. McKague, "Assessment of CYGNSS wind speed retrieval uncertainty," *IEEE J. Sel. Topics Appl. Earth Observ. Remote Sens.*, vol. 12, no. 1, pp. 87–97, Jan. 2019, doi: 10.1109/JSTARS.2018.2825948.

[5] R. Young and J. Vinoth, "An "extended fetch" model for the spatial distribution of tropical cyclone wind-waves as observed by altimeter," *Ocean Eng.*, vol. 70, pp. 14–24, Sep. 2013, doi: 10.1016/ j.oceaneng. 2013.05.015.

[6] P. A. Hwang and Y. Fan, "Effective fetch and duration of tropical cyclone wind fields estimated from simultaneous wind and wave measurements: Surface wave and air-sea exchange computation," *J. Phys. Oceanogr.*, vol. 47, pp. 447–470, Feb. 2017.

[7] V. N. Kudryavtsev, V. K. Makin, and B. Chapron, "Coupled sea surface-atmosphere model 2. Spectrum of short wind waves," *J. Geophys. Res.*, vol. 104, no. C4, pp. 7625–7639, Apr. 1999, doi: org/10.1029/1999JC900005.

[8] T. Elfouhaily, B. Chapron, K. Katsaros, and D. Vandemark, "A unified directional spectrum for long and short wind-driven waves," *J. Geophys. Res.*, vol. 102, no. C7, pp. 15781–15796, Jul. 1997, doi: org/10.1029/97JC00467.

[9] P. A. Hwang, D. M. Burrage, D. W. Wang, and J. C. Wesson, "An advanced roughness spectrum for computing microwave L-band emissivity in sea surface salinity retrieval," *IEEE Geosci. Remote Sens. Lett.*, vol. 8, no. 3, pp. 547–551, May 2011, doi: 10.1109/ LGRS.2010.2091393.

[10] M. D. Anguelova and P. W. Geiser, "Microwave emissivity of sea foam layers with vertically inhomogeneous dielectric properties," *Remote Sens. Environ.*, vol. 139, pp. 81–96, Aug. 2013.

[11] F. D. Hastings, J. B. Schneider, and S. L. Broschat, "A Monte-Carlo FDTD technique for rough surface scattering," *IEEE Trans. Antennas Propag.*, vol. 43, no. 11, pp. 1183–1191, Nov. 1995.

[12] J. Li, L.-X. Guo, and H. Zeng, "FDTD investigation on electromagnetic scattering from two-layered rough surfaces under UPML absorbing condition," *Chin. Phys. Lett.*, vol. 26, no. 2, 2009, Art. no. 034101.

[13] J. Li, L.-X. Guo, H. Zeng, and X.-B. Han, "Message-passing-interface-based parallel FDTD investigation on the EM scattering from a 1-D rough sea surface using uniaxial perfectly matched layer absorbing boundary," *J. Opt. Soc. Amer. A*, vol. 26, no. 6, pp. 1494–1502, Jun. 2009.

[14] J. Li, L.-X. Guo, Y.-C. Jiao, and C.-G. Jia, "Frequency response of 1D dispersive sea surface by the ADE-FDTD method," *Waves Random Complex Media*, vol. 22, no. 2, pp. 305–316, 2012.

[15] A. K. Fung, M. R. Shah, and S. Tjuatja, "Numerical simulation of scattering from three-dimensional randomly rough surfaces," *IEEE Trans. Geosci. Remote Sens.*, vol. 32, no. 5, pp. 986–994, Sep. 1994.

[16] J. Li, L.-X. Guo, and H. Zeng, "FDTD investigation on electromagnetic scattering from two-dimensional layered rough surfaces," *ACES J.*, vol. 25, no. 5, pp. 450–457, May 2010.

[17] L. Kuang and Y-Q Jin, "Bistatic scattering from a three-dimensional object over a randomly rough surface using the FDTD algorithm," *IEEE Trans. Antennas Propag.*, vol. 55, no. 8, pp. 2302–2312, Aug. 2007.

[18] J. Li, L.-X. Guo, and H. Zeng, "FDTD method investigation on the polarimetric scattering from 2-D rough surface," *Prog. Electromagn. Res.*, vol. 101, pp. 173–188, 2010.

[19] J. Li, L.-X. Guo and H. Zeng, "FDTD investigation on bistatic scattering from a target above two-layered rough surfaces under UPML absorbing condition," *Prog. Electromagn. Res.*, vol. 88, pp. 197–211, 2008.

[20] J. Li, L.-X. Guo and H. Zeng, "FDTD investigation on the electromagnetic scattering from a target above a randomly rough sea surface," *Waves Random Complex Media*, vol. 18, no. 4, pp. 641–650, Nov. 2008.

[21] J. Li, L.-X. Guo and H. Zeng, "Investigation of composite electromagnetic scattering from ship-like target on the randomly rough sea surface using FDTD method," *Chin. Phys. B*, vol. 18, no. 7, pp. 2757–2763, Jul. 2009.

[22] K. S. Yee, "Numerical solution of initial boundary value problems involving Maxwell's equations in isotropic media," *IEEE Trans. Antennas Propag.*, vol. 14, no. 3, pp. 302–307, May 1966.

[23] A. Taflove and S. C. Hagness, *Computational Electrodynamics: The Finite-Difference Time-Domain Method*. New York, NY, USA: IEEE Press, 2005.

[24] J. B. Schneider, "Understanding the finite-difference time-domain method," Accessed on: Sep. 7, 2017. [Online]. Available: http://www.eecs.wsu.edu/∼schneidj/ufdtd/ufdtd.pdf

[25] L. A. Klein and C. T. Swift, "An improved model for the dielectric constant of seawater at microwave frequencies," *IEEE J. Ocean. Eng.*, vol. 2, no. 1, pp. 104–111, Jan. 1977.

[26] M. D. Anguelova and M. H. Bettenhausen, "Effect of a sea spray layer on L-band signal from ocean surface," in *Proc. GNSS+R Workshop*, Ann Arbor, MI, USA, May 23–25, 2017. [Online]. Available: http://www.gnssr2017.org/images/Poster_session/GNSS+R2017_Poster_Scat_1_Anguelova_SprayLband.pdf. Accessed on: Sep. 30, 2018.

[27] R. S. Bortkovskii, *Air-Sea Exchange of Heat and Moisture During Storms*, E. C. Monahan, Ed. Dordrecht, The Netherlands: Reidel, 1987.

[28] J. Wu, "Individual characteristics of whitecaps and volumetric description of bubbles," *IEEE J. Ocean. Eng.*, vol. 17, no. 1, pp. 150–158, Jan. 1992.

[29] A. Voronovich, "Small-slope approximation for electromagnetic wave scattering at a rough surface of two dielectric half spaces," *Waves Random Media*, vol. 4, pp. 337–367, 1994.

[30] J. T. Johnson and M. Zhang, "Theoretical study of the small slope approximation for ocean polarimetric thermal emission," *IEEE Trans. Geosci. Remote Sens.*, vol. 37, no. 5, pp. 2305–2316, Sep. 1999, doi: 10.1109/36.789627.

[31] P. A. Hwang, "Foam and roughness effects on passive microwave remote sensing of the ocean," *IEEE Trans. Geosci. Remote Sens.*, vol. 50, no. 8, pp. 2978–2985, Aug. 2012, doi: 10.1109/TGRS.2011.2177666.

[32] A. Camps *et al.*, "The emissivity of foam-covered water surface at L-band: Theoretical modeling and experimental results from the FROG 2003 field experiment," *IEEE Trans. Geosci. Remote Sens.*, vol. 43, no. 5, pp. 925—937, May 2005.

[33] M. Goodberlet and I. PopStefania, "Retrievals of wind and rain rate from combined measurements of up-looking and down-looking SFMRs," presented at the 67th Interdept. Hurricane Conf., College Park, MD, USA, Presentation 05-S7, Mar. 5–7, 2013. [Online]. Available: https://www.ofcm.gov/meetings/TCORF/ihc13/67IHC-Linking-File.htm. Accessed on: Jul. 5, 2019.

[34] D. W. Wang and H. W. Wijesekera, "Observations of breaking waves and energy dissipation in modulated wave groups," *J. Phys. Oceanogr.*, vol. 48, no. 12, pp. 2937–2948, 2018.

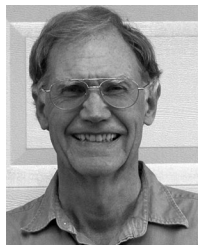

Derek M. Burrage was born in Melbourne, VIC, Australia, in 1951. He received the B.Sc. (geophysics) degree from the University of Melbourne, Melbourne, VIC, Australia, in 1971, and the Ph.D. (oceanography) degree from the University of Delaware, Newark, DE, USA, in 1986.

From 1986 to 2001, he was a Research Scientist with the Australian Institute of Marine Science, Townsville, QLD, Australia. From 2001 to 2003, he was an Associate Research Scientist with the Department of Marine Science, University of Southern Mississippi, Stennis Space Center (SSC), MS, USA, and under contract to the U.S. Naval Research Laboratory (NRL). He transitioned to the position of Oceanographer with NRL, SSC, in 2003, and retired in 2018. His expertise lies in physical oceanography, dynamics of regional seas, airborne and satellite infrared, and microwave remote sensing and computer simulation. He has authored or coauthored more than 25 journal articles and 30 conference and workshop proceedings papers, on topics ranging from regional ocean circulation, radar altimetry, and oceanographic radiometry and reflectometry, to EM simulation of ocean remote sensing instruments and associated signals. He recently led a four-year NRL project "Combined use of *L*-band reflectometry and radiometry to retrieve surface winds, waves, and wakes in tropical cyclones." His current interests include interactions of microwave radiation with the wind-roughened sea surface with applications to retrieving sea surface temperature, salinity, and wind fields using microwave radiometry and reflectometry. Since retiring from NRL on December 31, 2018, he has continued his research on microwave remote sensing and simulation.

Dr. Burrage is currently a member of the Extended Science Team for the Cyclone global navigation satellite system satellite mission.

Magdalena D. Anguelova received the B.S. degree in engineering physics from the University of Sofia, Sofia, Bulgaria, in 1984, and the M.S. and Ph.D. degrees in oceanography from the University of Delaware, Newark, DE, USA, in 1997 and 2002, respectively.

From 1984 to 1994, her experience in remote sensing was based on work with the Institute of Electronics, Bulgarian Academy of Sciences, Sofia, Bulgaria. She worked with diode lasers to monitor atmospheric pollution and with coherent Doppler Lidar to measure wind speed and direction in the atmosphere. She joined the Remote Sensing Division, U.S. Naval Research Laboratory, Washington, DC, USA, in 2002, as a National Research Council Postdoctoral Fellow. She was a Team Member of the four-year NRL project "Combined use of *L*-band reflectometry and radiometry to retrieve surface winds, waves, and wakes in tropical cyclones." Her research interests are in the physics and measurements of breaking waves, sea foam, bubbles and bubble clouds, sea spray aerosols, and air–sea fluxes of heat and gases. These topics motivate her work on using passive microwave remote sensing to obtain satellite retrievals of whitecap fraction and build a whitecap database that is useful to study the variability of whitecaps and surface fluxes and to parameterize various air–sea interaction processes.

Dr. Anguelova is a member of the American Geophysical Union and the American Meteorological Society.

David W. Wang received the B.S. and M.S. degrees from the National Cheng-Kung University, Tainan, Taiwan, in 1977 and 1979, respectively, and the Ph.D. degree in coastal and oceanographic engineering from the University of Florida, Gainesville, FL, USA, in 1986.

Since 1999, he has been a Research Oceanographer with the Oceanography Division at Naval Research Laboratory, Stennis Space Center, MS, USA. During 2015 to 2018, he was a Team Member of the four-year NRL project "Combined use of *L*-band reflectometry and radiometry to retrieve surface winds, waves, and wakes in tropical cyclones." His research interests include air–sea interaction dynamics, surface wave measurements and analysis, and buoy wave system developments.

Joel C. Wesson received the B.A. degree in physics from Swarthmore College, Swarthmore, PA, USA, in 1982, and the Ph.D. degree in physical oceanography from the University of Washington, Seattle, WA, USA, in 1991.

From 1992 to 1995, he was a Researcher with McGill University, and from 1995 to 1997, a National Research Consortium Post-Doc with the Naval Research Laboratory (NRL), Stennis Space Center. He joined NRL as an Oceanographer in 2000. He was also a Team Member of the four-year NRL project "Combined use of *L*-band reflectometry and radiometry to retrieve surface winds, waves, and wakes in tropical cyclones." His expertise lies in instrument development, airborne and satellite oceanography, and small-scale turbulent ocean processes and ocean measurements. He has authored or coauthored more than 12 journal articles and 14 conference and workshop proceedings papers on topics ranging from wave bubble measurement and microstructure instruments to turbulence and radiometry observations of the ocean. His current focus is on Flying Sea Glider development.